Quantifying Turbulence-Induced Segregation of Inertial Particles

Enrico Calzavarini,[1,*] Massimo Cencini,[2] Detlef Lohse,[1] and Federico Toschi[3]

(International Collaboration for Turbulence Research)

[1]*Department of Applied Physics, JMBC Burgers Center for Fluid Dynamics, and IMPACT Institute, University of Twente,
P.O. Box 217, 7500 AE Enschede, The Netherlands*
[2]*INFM-CNR, SMC Department of Physics, Università "La Sapienza," Piazzale Aldo Moro 2, 00185 Roma, Italy,
and CNR-ISC, Via dei Taurini 19, 00185 Roma, Italy*
[3]*CNR-IAC, Viale del Policlinico 137, 00161 Roma, Italy, and INFN, Sezione di Ferrara, via Saragat 1, 44100 Ferrara, Italy*

Particles with different density from the advecting turbulent fluids cluster due to the different response of light and heavy particles to turbulent fluctuations. This study focuses on the quantitative characterization of the *segregation* of dilute polydisperse inertial particles evolving in turbulent flow, as obtained from direct numerical simulation of homogeneous isotropic turbulence. We introduce an indicator of segregation amongst particles of different inertia and/or size, from which a length scale r_{seg}, quantifying the segregation degree between two particle types, is deduced.

PACS numbers: 47.27.−i, 47.10.−g

The ability of efficiently mixing transported substances is one of the most distinctive properties of turbulence, which is ubiquitous in geophysical and astrophysical fluids. New features appear when turbulent flows are seeded with finite-size particulate matter having density ρ_p different from the carrier fluid density ρ_f. Because of inertia, measured by the Stokes time $\tau = a^2/(3\beta\nu)$ [a being the particle radius and ν the fluid viscosity; $\beta = 3\rho_f/(2\rho_p + \rho_f)$], such particles detach from fluid parcels' paths and distribute inhomogeneously [1–3]. Although this phenomenon of *preferential concentration* [4] has been known for a long time [1,2], it continues to attract much attention (see [3,5–11] and references therein). It is important for drag reduction by microbubbles [12], for the effects of microbubbles on the small scales of turbulence [13], for aerosol physics which is critical for climatological models [14], or for understanding the patchiness of chemical and biological agents in the oceans [15]. The key issue is the tendency of inertial particles to form clusters with the consequent enhancement of the particle interaction rate.

When having *different* particle types in the same flow (polydispersity), the respective particles probe different flow structures: light particles ($\beta > 1$, e.g., air bubbles in water) preferentially concentrate in high vorticity regions, while heavier ones ($\beta < 1$, e.g., sand grains in water) are expelled by rotating regions. This leads to a *segregation* of the different particle types, which intuitively is characterized by some *segregation length scale*. An example of particle segregation is shown in Fig. 1, where snapshots of light and heavy particles' positions are depicted. The segregation length depends on both the respective particle densities and Stokes numbers $\text{St} = \tau/\tau_\eta$, which measure the particle response time τ in units of the Kolmogorov time τ_η (characterizing the smallest active time scale of turbulence). This Letter aims to systematically *quantify* the segregation length as a function of both the relative density (β) and the Stokes number, which together characterize the particle classes.

To demonstrate our method, we consider a model of passively advected dilute (to neglect collisions) suspensions of particles in homogeneous, isotropic turbulence. Particles are described as material points which are displaced by both inertial forces (pressure-gradient force, added mass) and viscous forces (Stokes drag). Additional physical effects (such as lift force, history force, buoyancy, or finite-size and finite-Reynolds corrections), which may becomes important for the cases of light and/or large particles ($\beta\text{St} \geq 1$), are here neglected for simplicity.

The particle dynamics then reads [16,17] (see also [18])

$$d_t\boldsymbol{x} = \boldsymbol{v}, \qquad d_t\boldsymbol{v} = \beta D_t\boldsymbol{u} + \tau^{-1}(\boldsymbol{u} - \boldsymbol{v}), \qquad (1)$$

where $\boldsymbol{x}$, $\boldsymbol{v}$ denote the particle position and velocity, respectively, and $d_t = \partial_t + \boldsymbol{v} \cdot \nabla$ is the time derivative along the particle path. The incompressible fluid velocity $\boldsymbol{u}$ evolves according to the Navier-Stokes equations:

$$D_t\boldsymbol{u} = \partial_t\boldsymbol{u} + \boldsymbol{u} \cdot \nabla\boldsymbol{u} = -\nabla p/\rho_f + \nu\Delta\boldsymbol{u} + \boldsymbol{f}, \quad (2)$$
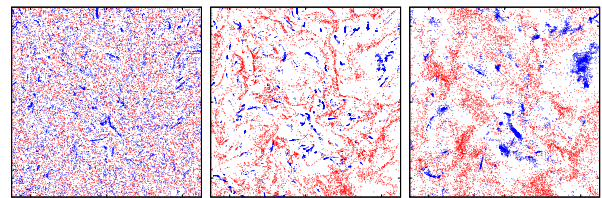

FIG. 1 (color online). Slice $400\eta \times 400\eta \times 10\eta$ of heavy $\beta = 0$ (red or light gray) and light $\beta = 3$ (blue or dark gray) particle positions. From left to right: $\text{St} = 0.1$, 1, and 4.1. Data refer to the simulation at $\text{Re}_\lambda = 180$.

where p denotes the pressure and $\boldsymbol{f}$ is an external forcing injecting energy at a rate $\varepsilon = \langle \boldsymbol{u} \cdot \boldsymbol{f} \rangle$. Equation (2) is evolved by means of a 2/3-dealiased pseudospectral code with a second order Adams-Bashforth time integrator. The fluid velocity at particle position is evaluated by means of a three-linear interpolation. Simulations have been performed in a cubic box of side $L = 2\pi$ with periodic boundary conditions, and by using $N^3 = 128^3$ and 512^3 mesh points (reaching Taylor Reynolds numbers $\mathrm{Re}_\lambda = 75$ and 180). The respective Taylor length scales $\lambda \equiv \sqrt{\langle u_x^2 \rangle / \langle \partial_x u_x^2 \rangle}$ are $\lambda = 13\eta$ and 21η. The parameter space $\beta \times \mathrm{St} \in [0:3] \times [0:4]$ is sampled with 504 (β, St) points with $N = 10^5$ particles per type in the former case and 64 (optimally chosen by means of a Monte Carlo allocation scheme based on lower resolution results) with $N = 1.6 \times 10^6$ in the latter. Given the small Re_λ dependence, we will report here mostly results from $\mathrm{Re}_\lambda = 75$, for which we have a more complete sampling of the parameter space (β, St).

A requirement for any segregation indicator is to result in zero segregation length for any two statistically independent distributions of particles coming from the same class of particles, at least in the limit of infinitely many particles. If the observation scale is too small and the number of particle finite, even independent particle realizations of the same class of particles will artificially appear to be segregated. Therefore, the definition of segregation strictly requires one to indicate the observation scale r, and it will be sensitive to the particle number.

However, we aim at a robust observable. Classical and natural observables, as, e.g., the minimal distance between different type of particles, strongly depend on particle number and hence are not robust. Harmonic averages of particle distances could be sensitive to small scales and not be spoiled by the large scales, but the choice of the weight exponent is rather arbitrary. The use of a density correlation function $\langle \rho_1(x)\rho_2(x + r)\rangle$ [19], though possible, requires the introduction of a coarse-graining scale (to define the densities) which may quantitatively affect the estimate. The mixed pair correlation function, or mixed radial distribution function [20], is not bounded at small scales for clustered distributions of point particles.

Our approach is inspired by Kolmogorov's distance measure between two distributions [21] and is based on particle densities coarse grained over a scale r, which can be understood as resolution of a magnifying glass used to look at the segregation. The whole volume L^3 is partitioned into $\mathcal{M}(r) = (L/r)^3$ cubes. We then define the following segregation indicator:

$$S_{\alpha_1, \alpha_2}(r) = \frac{1}{N_{\alpha_1} + N_{\alpha_2}} \sum_{i=1}^{\mathcal{M}(r)} |n_i^{\alpha_1} - n_i^{\alpha_2}|. \qquad (3)$$

The subscripts α_1 and α_2 index the particle parameters, i.e., $\alpha_1 = (\beta_1, \mathrm{St}_1)$ and $\alpha_2 = (\beta_2, \mathrm{St}_2)$, N_α is the total number of particles of α-type, while n_i^α is that of particles contained in each cube i. The case $\alpha_1 = \alpha_2$ should be considered as taking independent realizations of the par-

ticle distribution (otherwise $S_{\alpha_1, \alpha_1} \equiv 0$ trivially) so that $S_{\alpha, \alpha}$ sets the minimum detectable segregation degree.

Let us first discuss the limiting cases of $S_{\alpha_1, \alpha_2}(r)$, which can vary in the range $[0, 1]$. $S_{\alpha_1, \alpha_2}(r) = 1$ means that the two distributions are not overlapping when looked at resolution r. For small enough scales, i.e., $r \ll 1/\rho^{1/3}$ (which is the mean distance of two particles with $\rho = N/L^3$ the particle number density) this holds for any realization, and therefore $\lim_{r \to 0} S_{\alpha_1, \alpha_2} = 1$. On the contrary, $\lim_{r \to L} S_{\alpha_1, \alpha_2} = 0$ as the total number of particles of the two species is globally identical (as assumed here). These limiting cases are observed in Fig. 2. Clearly, S_{α_1, α_2} is a meaningful indicator of segregation only if it does not depend too severely on the particle number N. Indeed, in Fig. 2, S_{α_1, α_2} (computed for the heavy and light particles' distribution of the central panel of Fig. 1) shows only a very weak N dependence at sufficiently large N. This is in contrast with the behavior of (3) for two independent and homogeneously distributed particle realizations (also shown in Fig. 2). The latter case can be easily understood recognizing that in each box of side r, n_i is a Poisson random variable, so that we can estimate $n_i \approx \rho r^3 \pm \sqrt{\rho r^3}$, where the two terms come from the average and the fluctuation contributions, respectively. In Eq. (3) the average cancels, and summing the fluctuations over all the $(L/r)^3$ cells, one has the order of magnitude estimate $S(r) \sim (L/r)^3 N^{1/2} (r/L)^{3/2} = N^{1/2} (r/L)^{-3/2}$, explaining both the observed scaling behavior and the strong dependence on N.

The segregation indicator allows us to extract the desired segregation length scale r_{seg}. This can be done by fixing an arbitrary threshold value for S; we employed $S_{\alpha_1, \alpha_2}(r_{\mathrm{seg}}) = 1/2$ (see Fig. 2). With this definition, as shown in the inset
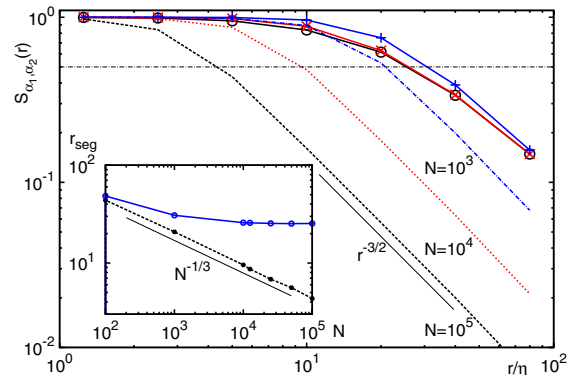

FIG. 2 (color online). $S_{\alpha_1, \alpha_2}(r)$ vs r for $\alpha_1 = (\beta_1 = 0, \mathrm{St}_1 = 1.1)$ (heavy type) and $\alpha_2 = (\beta_2 = 3, \mathrm{St}_2 = 1.1)$ (light type) for different particle numbers $N(= N_{\alpha_1} = N_{\alpha_2})$: (○) $N = 10^5$, (×) $N = 10^4$, and (+) $N = 10^3$. Dashed and dotted lines refer to homogeneously distributed particles samples at various N. The expected Poisson scaling behavior, $S_{\alpha_1, \alpha_2} \propto r^{-3/2}$, is also reported. Inset: r_{seg}, defined by $S_{\alpha_1, \alpha_2}(r_{\mathrm{seg}}) = 1/2$, as a function of N for both heavy vs light particles cases and Poissonian samples. While for the former r_{seg} saturates as N increases, for the latter r_{seg} goes to zero like $r_{\mathrm{seg},h} \propto N^{-1/3}$, as expected for Poissonian samples (see text for details).

of Fig. 2, for truly segregated (heavy vs light) samples $r_{\rm seg}$ saturates with increasing N. This does not hold for uniformly distributed (nonsegregated) particles. In the latter case $r_{\rm seg}$ essentially coincides with the interparticle distance $r_{\rm seg} = r_{\rm seg,h} \approx 1/\rho^{1/3} = L/N^{1/3}$, as also seen from the inset of Fig. 2. The behavior of $r_{\rm seg}$ encompasses the fact that for a finite number of particles N a natural cutoff distance exists (the mean interparticle distance) although we know theoretically that $\lim_{N\to\infty} r_{\rm seg}(N) = 0$. Hence $r_{\rm seg,h}(N)$ can be interpreted as the accuracy in estimating $r_{\rm seg}$ given a finite particle number N.

We now calculate $r_{\rm seg}$ for a pair of two different particle classes to quantify their mutual segregation. Figure 3 displays $S_{\alpha_1,\alpha_2}(r)$ for distributions composed of heavy particles with $\beta_1 = 0$ and $St_1 = \mathcal{O}(1)$ and particles with the same $St(= St_2 = St_1)$ but different densities. As one can see, segregation increases with the density difference, but $r_{\rm seg} \approx r_{\rm seg,h}$ for $\beta_2 < 0.5$, meaning that heavy enough particles basically all visit the same locations in the flow, irrespective of their exact density: They tend to avoid vortical regions [8]. A sensitive increase of $r_{\rm seg}$ is observed for $\beta_2 > 1$ (Fig. 3, inset), and as expected the maximal segregation length is obtained for bubbles, i.e., particles with density ratio $\beta = 3$, where $r_{\rm seg} \approx 25\eta \approx 1.9\lambda$. For the same case, $St = 1.1$, $\beta = 0$ vs $\beta = 3$, at $Re_\lambda = 180$ we find $r_{\rm seg} \approx 29\eta \approx 1.4\lambda$.

Thanks to the large number of particle types in our database we can extend the study of the segregation length to a wide range of physical parameters. In Fig. 4 we show the value of the segregation length by fixing $\alpha_1 = (\beta_1, St_1) = (0, 1.1)$ (left panel), the heavy particles of the middle panel of Fig. 1 or the light ones by fixing $\alpha_1 = (3, 1.1)$ (right panel), and varying $\alpha_2 = (\beta_2, St_2)$ for the second kind of particles. The emerging picture is as follows. Particle class pairs with $St_1 \approx St_2$ and $\beta_1 \approx \beta_2$ have a segregation length close to the interparticle distance $r_{\rm seg,h}$

and are unsegregated, while as soon as the Stokes number or the density difference become larger, $r_{\rm seg} > r_{\rm seg,h}$. The maximal segregation length $(r_{\rm seg}^{\rm (max)} \approx 27\eta \approx 2.1\lambda)$ is roughly twice the Taylor microscale and is realized for particles with large density difference $\beta_1 = 0$ and $\beta_2 > 1$ (or $\beta_1 = 3$ and $\beta_2 < 1$). These results thus confirm those of Fig. 3. It is interesting to note that heavy couples, β_1, $\beta_2 \lesssim 1$, segregate less than light ones, β_1, $\beta_2 \gtrsim 1$, which are thus much more sensitive to small variations of density and/or response times. The correlation between position and flow structure is thus much stronger for light particles.

We next systematically study what happens when fixing St or β. In the first four panels (from left to right) of Fig. 5, $r_{\rm seg}$ is shown as a function of β_1 and β_2, where we fixed the Stokes numbers, $St_1 = St_2 = St = (0.31, 0.6, 1.1, 4.1)$. Close to the diagonal $\beta_1 \approx \beta_2$, it is $r_{\rm seg} \lesssim r_{\rm seg,h}$; i.e., similar particles are poorly segregated. Outside these regions $r_{\rm seg} > r_{\rm seg,h}$, and segregation is above the accuracy threshold $r_{\rm seg,h}$. Two observations are in order. First, the strongest segregation is present for the case of $St \sim 1$, meaning that response times of the order of the Kolmogorov time are best suited to generate strong correlations between flow structures and particle positions and consequently segregation. Further, segregation is stronger for couples composed by very heavy ($\beta \sim 0$) and very light ($\beta \sim 3$) particles. Therefore, light and heavy particles with $St \sim 1$ display the strongest clusterization. Second, the numerical value of the segregation length saturates to a constant value $\approx 2\lambda$, strongly indicating that we are measuring an intrinsic property of the underlying turbulent flow emerging when particles are strongly clusterized.

The two rightmost panels of Fig. 5 display cuts done by fixing the density, namely, $\beta_1 = \beta_2 = \beta = 1.5$ (and $= 3$). For $\beta < 1.5$, i.e., relatively heavy or weakly light particles, there is only a slight tendency toward segregation at varying the Stokes number. This means that even if the particles form clusters, such clusters are not too sensitive against variation of St. For very light particles, $\beta = 3$, the situation
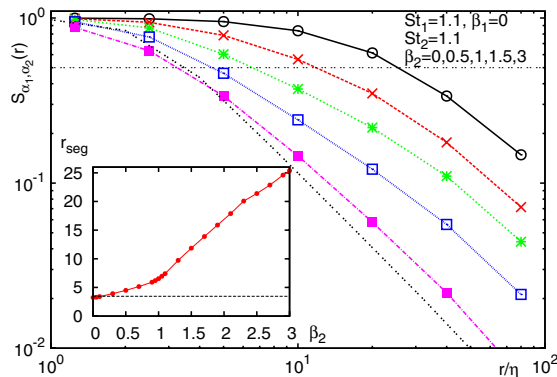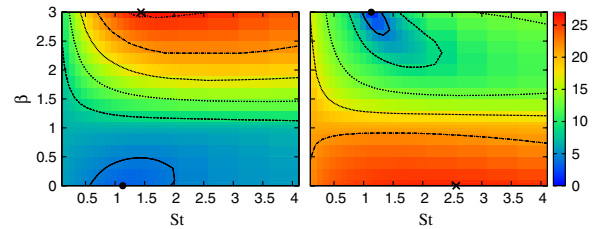

FIG. 3 (color online). $S_{\alpha_1,\alpha_2}(r)$ for $\alpha_1 = (\beta_1 = 0, St_1 = 1.1)$ and $\alpha_2 = (\beta_2, St_2 = St_1)$, i.e., a heavy particle with $\beta_1 = 0$ and a given St vs those having the same St but different densities β_2. From bottom to top: $\beta_2 = 0, 0.5, 1, 1.5, 3$. Inset: $r_{\rm seg}$ vs β_2, with $r_{\rm seg}$ defined as in Fig. 2, i.e., $S_{\alpha_1,\alpha_2}(r_{\rm seg}) = 1/2$. The straight dashed line shows $r_{\rm seg,h} \approx 4\eta \approx 0.3\lambda$.

FIG. 4 (color online). $r_{\rm seg}$ between particle distributions with $\beta = 0$, $St = 1.1$ (left panel) and $\beta = 3$, $St = 1.1$ (right panel) vs distributions with generic β, St. (●) indicates the reference particle type, and (×) the location of the maximal segregation length $r_{\rm seg}^{\rm (max)}$. The solid contour line, traced at $r_{\rm seg} = r_{\rm seg,h} \equiv L/N^{1/3}$, sets the sensitivity level to distinguish between segregated and unsegregated particle distributions. Dashed and dotted lines are drawn at $r_{\rm seg} = nr_{\rm seg,h}$, with $n = 2, ..., 6$. The color scale codes the value of $r_{\rm seg}$ in units of the Kolmogorov length, η.
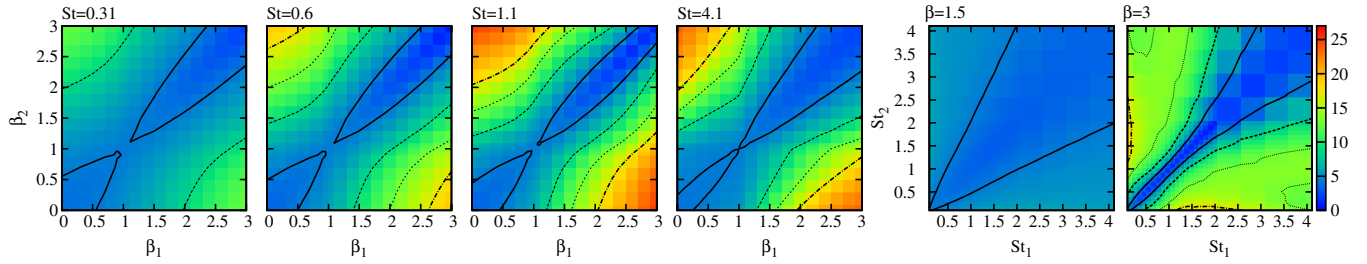
FIG. 5 (color online).   From left to right, segregation length r_{seg} between distribution of particles with St = (0.31, 0.6, 1.1, 4.1) vs the densities β_1, β_2 and (last two panels) for particle class pairs having the same densities $\beta_1 = \beta_2 = 1.5$ (and = 3) and different St. The color scale and the contour lines are, as in Fig. 4, at $r_{\text{seg}} = n r_{\text{seg},h}$, with $n = 2, \ldots, 4$.

is different when comparing the case of St $\sim$ 1 with the case of St $\sim$ 0. As expected for St $\sim$ 0, though particles are light, they distribute almost uniformly (they are not too far from the tracer limit), while for St $\geq$ 1 they are strongly correlated with the vortex filaments which are unevenly distributed in the flow [22].

In conclusion, we introduced an indicator able to quantify the segregation degree and to allow the definition of a segregation length scale r_{seg} between different classes of particles, which follow simplified dynamical equations in isotropic turbulence. The extracted information is in line with the intuitive idea of expulsion and/or entrapment of particles due to vortical structures, which is now on a more quantitative ground. The maximal segregation length, for instance for heavy particles ($\beta = 0$, St = 1.1), is obtained with bubbles with slightly larger Stokes (St $\sim$ 1.4) (Fig. 4, leftmost panel); it measures $r_{\text{seg}}^{(\text{max})} \simeq 27\eta \simeq 2.1\lambda$ at Re$_\lambda$ = 75. At Re$_\lambda$ = 180, similarly we get $r_{\text{seg}}^{(\text{max})} \simeq 48\eta \simeq 2.3\lambda$. Therefore, $r_{\text{seg}}^{(\text{max})}$ is about twice the Taylor length.

Important areas of application of the developed methods go far beyond homogeneous isotropic turbulence, including, e.g., heterogeneous catalysis or flotation, where one is interested in the collision probability of argon bubbles and solid contaminations in turbulent liquid steel [23]. In this context our finding that $r_{\text{seg}}^{(\text{max})} \simeq 2\lambda$ suggests that the cleaning could become less efficient at high Re$_\lambda$, as bubbles and particles then become more segregated. However, a quantitative statement requires better models for both the flow geometry and the effective particle force. Another example for the application of the suggested method is the formation of rain drops at solid nuclei in clouds [19], a mechanism which is crucial to develop models for rain initiation [6]. Disregarding particle segregation in all these examples would lead to estimates of the collision rate which could be orders of magnitude off. We have already observed that the point-particle model adopted in our study neglects some hydrodynamical effects which corresponds to additional forces in the particle equation. Such forces, when included with proper modeling, might smooth the intensity of segregation which, as we have shown, is mainly due to the relative strength of inertial forces.

Finally, we stress that the introduced segregation indicator can be employed in all phenomena involving differ-ent classes of segregating objects. Provided one knows the position of all the objects, no prior knowledge on the physical mechanism which leads to segregation is needed. Unprocessed data of this study are publicly available at the iCFDdatabase [24]

*Present address: École Normale Supérieure de Lyon, CNRS UMR5672, 46 Allée d' Italie, 69007 Lyon, France.
[1] M. Maxey, J. Fluid Mech. **174**, 441 (1987).
[2] A. Crisanti *et al.*, Phys. Fluids A **4**, 1805 (1992).
[3] E. Balkovsky *et al.*, Phys. Rev. Lett. **86**, 2790 (2001).
[4] J. Eaton and J. Fessler, Int. J. Multiphase Flow **20**, 169 (1994).
[5] J. Bec *et al.*, Phys. Fluids **17**, 073301 (2005).
[6] M. Wilkinson *et al.*, Phys. Rev. Lett. **97**, 048501 (2006).
[7] S. Ayyalasomayajula *et al.*, Phys. Rev. Lett. **97**, 144507 (2006).
[8] J. Bec *et al.*, Phys. Rev. Lett. **98**, 084502 (2007).
[9] I. Mazzitelli *et al.*, J. Fluid Mech. **488**, 283 (2003).
[10] J. Bec, Phys. Fluids **15**, L81 (2003).
[11] E. Calzavarini *et al.*, J. Fluid Mech. **607**, 13 (2008).
[12] T. H. van den Berg *et al.*, Phys. Rev. Lett. **94**, 044501 (2005).
[13] J. Rensen *et al.*, J. Fluid Mech. **538**, 153 (2005).
[14] A. Ackerman *et al.*, Nature (London) **432**, 1014 (2004).
[15] R. Reigada *et al.*, Proc. R. Soc. B **270**, 875 (2003).
[16] M. Maxey and J. Riley, Phys. Fluids **26**, 883 (1983).
[17] T. Auton *et al.*, J. Fluid Mech. **197**, 241 (1988).
[18] A. Babiano *et al.*, Phys. Rev. Lett. **84**, 5764 (2000).
[19] G. Falkovich *et al.*, Nature (London) **419**, 151 (2002).
[20] Y. Zhou, A. S. Wexler, and L.-P. Wang, J. Fluid Mech. **433**, 77 (2001).
[21] A. N. Kolmogorov, Sankhya: Indian J. Stat. A **25**, 159 (1963).
[22] J. Jimenez and A. A. Wray, J. Fluid Mech. **373**, 255 (1998).
[23] L. F. Zhang and S. Taniguchi, Int. Mater. Rev. **45**, 59 (2000).
[24] http://cfd.cineca.it.